Volume 1 | Number 1 | Jan 2013 | Pages 1–100

Nanoscale

www.rsc.org/nanoscale

ROYAL SOCIETY
OF CHEMISTRY

This is an *Accepted Manuscript*, which has been through the Royal Society of Chemistry peer review process and has been accepted for publication.

Accepted Manuscripts are published online shortly after acceptance, before technical editing, formatting and proof reading. Using this free service, authors can make their results available to the community, in citable form, before we publish the edited article. We will replace this *Accepted Manuscript* with the edited and formatted *Advance Article* as soon as it is available.

You can find more information about *Accepted Manuscripts* in the **Information for Authors**.

Please note that technical editing may introduce minor changes to the text and/or graphics, which may alter content. The journal's standard **Terms & Conditions** and the **Ethical guidelines** still apply. In no event shall the Royal Society of Chemistry be held responsible for any errors or omissions in this *Accepted Manuscript* or any consequences arising from the use of any information it contains.

ROYAL SOCIETY
OF CHEMISTRY

www.rsc.org/nanoscale

Graphene Growth under *Knudsen* Molecular Flow on Confined Catalytic Metal Coil

Hyojin Bong[†], Sae Byeok Jo[†], Boseok Kang, Seong Kyu Lee, Hyun Ho Kim, Seung Goo Lee, Kilwon Cho*

Department of Chemical Engineering, Pohang University of Science and Technology, Pohang 790-784, Korea.

[†] H.Bong and S.B. Jo contributed equally to this work.

Abstract

We have established a simple method for drastically improving the productivity of chemical vapor deposition in large-area graphene synthesis by using a roll-stacked Ni coil as a catalyst. Our systematic investigation of the effects of a confined catalytic geometry has shown that the gas flow through interfacial gaps within the stack follows non-continuum fluid dynamics when the size of the gap decreases sufficiently, which enhances the dissolution of the carbon sources into the catalyst during synthesis. Quantitative criteria for graphene growth in the confined geometry are established through the introduction of the *Knudsen* number, *Kn*, which is the ratio of the mean-free-path of the gas molecules to the size of the gap. The criteria provided in this article for the synthesis of graphene in the confined geometry are expected to provide the foundations for the efficient mass production of large-area graphene. We also show that the evolution of the catalytic Ni surface in a stacked system results in larger grains in the (111) plane, and consequently in reproducible, uniform, and high-quality multi-layer graphene.

Keywords: Graphene, Graphene growth, Confined growth, *Knudsen* molecular flow, metal coil

2

Introduction

Graphene consists of two-dimensional carbon atoms with sp^2 bonds; it has excellent mechanical,[1] thermal,[2] optical,[3] and electrical properties.[4-7] There are many methods for the synthesis of graphene including the mechanical exfoliation of graphite,[8] epitaxial growth on SiC,[9-12] and chemical vapor deposition (CVD).[13-15] The CVD of hydrocarbon gases onto a sheet of a transition-metal catalyst produces graphene that possesses high quality, large sheet size, and transferability to arbitrary substrates. However, the dimensions of the resulting graphene sheet are constrained by the surface area of the metal catalyst, which sets limits on large-area graphene synthesis.[13, 15-18]

To obtain large-area graphene by CVD, the synthetic process must be organized, including the synthesis of graphene and consecutive transfer to arbitrary substrates. In a previous study, a 30 inch Cu foil was used for large-area graphene synthesis, and the acquired graphene was easily transferred to various substrates by using a simple wet-transfer method with a polymer supporting layer.[16] However, this process requires the foils to be separated from each catalytic surface, because the synthesis temperature (900~1000°C) is close to the melting point of Cu (1085°C) so that Cu surfaces in close proximity can easily weld together. Therefore, the size of a CVD chamber depends on the required graphene sheet size; the size of the chamber must be increased to achieve larger graphene. A continuous synthetic method, such as the roll-to-roll (R2R) based CVD process, has been demonstrated to scale up the graphene synthesis.[19] The R2R process does not require simultaneous heating of the entire catalyst surface, so the simple unrolling of a catalytic metal coil enables the synthesis of graphene sheets up to 100 m in length,[19] and also continuous transfer to flexible substrates.[16] However, in continuous synthetic methods, it is easily overlooked that the required deposition time and the thermal

energy consumption increase in proportion to the area of the graphene, which is critical to the efficient synthesis of large-area graphene.

To resolve these disadvantages while preserving the promising characteristics of both the conventional one-pot synthesis process and the continuous R2R process,[20, 21] an approach that enables the incorporation of various catalyst geometries such as a catalyst stacking with appropriate spacing for efficient spatial usage of the chamber needs to be developed. Moreover, for the stacked catalyst geometry, more sophisticated considerations of the gas flow behavior are required than for a conventional open non-stacked system. In this confined catalytic system, gas flows through narrow gaps between the catalytic surfaces, so the gas flow behavior and surface reactions on the catalyst surfaces are different from those in the open non-stacked system. Previous research has studied the mass transport of carbon sources in the CVD of graphene by using the boundary layer concepts of fluid mechanics.[22-25] However, these concepts could not be applied to this confined gap system, because the gas flow does not follow the conventional continuum-flow regime including the boundary layer concepts when the gap size is on the micron scale. Under these conditions, the flow changes to a non-continuum regime since viscous force exerted on each wall becomes dominant as the dimension of the fluidic system decreases. In the non-continuum regime, each individual gas molecule collides more frequently with the walls of the stack than with other gas molecules. Thus, the gas flow in the confined geometry should be described with a quantity that takes into account the dimensions of the system. Therefore, the *Knudsen* number, *Kn*, which is the ratio of the molecular mean free path to the characteristic dimension of the system, was recommended as a new parameter that takes into account the interfacial gap size. Taking the above considerations into account, we designed an efficient synthetic method in which a roll-

stacked catalytic metal coil is incorporated into the one-pot CVD process to simultaneously

maximize the catalytic area and minimize unnecessary time and energy consumption.

Moreover, we also thoroughly investigated the graphene growth mechanism for the confined

catalytic surface with this unconventional geometry. We used thermally evaporated Ni

(melting point 1453°C) substrate on a flexible stainless steel (SUS) and Si wafer to prevent

the catalyst sheets from sticking together during the process. Graphene grown on the roll-

stacked Ni catalytic coil has reproducible, uniform properties. We also constructed a system

consisting of stacked substrates as a simplified model of the roll-stacked Ni coil, and

systematically studied the mass transport mechanism in the stacked system. Quantitative

criteria for graphene growth in the confined geometry under a specific flow regime were

determined. Moreover, the metal catalyst surface quality was analyzed to determine how the

gap size in the stacked system affects the properties of the synthesized graphene.

Experimental section

Graphene growth

To fabricate a roll-stacked Ni/SUS coil, a 500 nm SiO_2 layer was deposited by PECVD and

then a 400 nm Ni film was deposited by thermal evaporation onto the stainless steel (SUS)

substrate. In the multi-layer or two-layer stacked systems, 400 nm Ni layers were deposited

onto each SiO_2/Si substrates (300 nm SiO_2) by using a thermal evaporator. Ni sources (purity

> 99.995%) were purchased from Alfa Aesar®. The Ni-evaporated substrates were loaded

into an inner quartz tube (diameter 1") inside a chemical vapor depositor under vacuum.

When the temperature of the furnace reached 900°C, the substrates were moved into it

rapidly and a flow of mixed gases was introduced through a tube. The mixed gases consisted

of methane, hydrogen and argon; the CH_4 gas flow rate was adjusted from 2 to 70 sccm (H_2 : Ar = 100:500 sccm), which corresponds to a CH_4 concentration in the range 0.33% to 10.45%. After 10 minutes of growth, the substrates bearing graphene were removed from the furnace quickly and cooled to room temperature in hydrogen gas.

Graphene transfer

To transfer a graphene film to an arbitrary substrate such as a SiO_2/Si wafer or glass, polymethyl methacrylate (PMMA) was coated onto the graphene grown on the Ni surface as a supporting layer. The SiO_2 layer was etched out with dilute HF and the Ni film was etched out with $FeCl_3$. The graphene/PMMA film was washed in deionized water to remove the etchant, then transferred to the substrate. Finally, we used chloroform to remove the PMMA.

Gap fabrication

To adjust the gap sizes, we fabricated trench structures with the SiO_2/Si wafers. First, the SiO_2 layer was removed by using HF and 2 mm ridges were left on both sides of the wafers. Then, the Si layer was etched by using a mixed solution of HF and HNO_3 (1:3 vol/vol). By varying the etching time, we obtained gap sizes of 520 nm and 30 μm. The gap sizes of 600 μm and 1.2 mm were obtained by placing one and two 600 μm thick wafer pieces between substrates.

Characterization

The morphologies of the graphene films were characterized with an optical microscope (Axioplan, Zeiss). Raman spectroscopy was conducted at a wavelength of 532 nm (WITec, Micro Raman). The film transmittances were determined by using UV-visible irradiation in transmittance mode. The sheet resistances were determined with a four-point probe tester. The Ni morphologies were obtained by using an atomic force microscope (Digital

Instruments Multimode Nanoscope III) in tapping mode. Normal mode X-ray diffraction (XRD) measurements were performed (wavelength 0.108 nm) at the Pohang Accelerator Laboratory (PAL) in Korea. Electron Backscatter Diffraction (EBSD) was installed on a focused ion beam (FEI Helios, Pegasus). EBSD analyses were performed with a step size of 5 nm, and the data were post-processed by using TSL® OIM 5.0 software.

Results and Discussion

1. CVD on roll-stacked coils

The use of a roll-stacked catalyst coil is a simple and effective method for synthesizing large-area graphene. Ni is an appropriate catalyst for roll-stacked coils because its melting point is much higher than the process temperature. Ni thin films were obtained by thermal evaporation onto one side of the flexible SUS foils and graphene was prepared on the Ni surfaces, as shown in Figure 1a. The use of Ni thin films enables the control of the number of layers in the graphene film, because less carbon dissolves in thin Ni films than in thick Ni foils.[13, 26, 27] CVD-grown graphene was grown under the flow of 1.64 vol% CH_4 gas (H_2:Ar:CH_4 = 100:500:10 sccm) at 900 °C for 10 min, then transferred onto various substrates. As a demonstration, we could obtain a 8 cm × 3 cm (width × length) graphene film in one-pot CVD synthesis by using a roll-stacked catalytic coil with effective dimension of 1 cm × 3 cm (diameter × length), which, beyond doubt, greatly enhanced the productivity of graphene CVD synthesis. Figure 1c shows optical images of graphene films obtained from the catalytic coil, which was transferred onto 300 nm SiO_2/Si wafers. Interestingly, we found that graphene grew only in the stacked surface region, in which the Ni surfaces faced the bare

SUS surfaces ($1^{st} \sim 4^{th}$ turns) but not in the non-stacked surface region where the Ni surface was open to free gas flow (Figure 1b).

2. CVD on multi-stacked substrates

To investigate the growth of graphene on Ni films in a confined geometry, 6 Ni-evaporated flat Si/SiO$_2$ substrates were stacked in a CVD chamber, as shown schematically in Figure 2a. The Ni surface on the substrate of the 0th layer was exposed to the free gas flow and the $1^{st} \sim 5^{th}$ layers were covered by other substrates. Because the Ni film surface are not perfectly flat, we estimated the gap size between the stacked substrates as 135 nm. Since both Si and Fe (SUS) possess high melting temperatures (1414 °C and 1538 °C, respectively) than the growth temperature (900°C), the roll-stacked and multi-stacked catalyst systems could be considered analogous except for the interfacial gap size (200 nm for roll-stacked system) estimated by the physical roughnesses of two facing surfaces. (Figure S2) The effect of gap sizes will be discussed in detail in the section 3.1.

As in the roll-stacked system, graphene grew only on the stacked surfaces (the $1^{st} \sim 5^{th}$ layers) other than exposed, non-stacked surfaces (0th layer) under the flow of 1.64 vol% CH$_4$ gas. To assess the quality of the synthesized graphene films, the films were transferred to 300 nm thick SiO$_2$/Si wafers as shown in Figure 2b. The number of layers in each graphene film was identified from the color contrast in the optical images:[28] the color darkened as the number of graphene layers increased, as shown in this figure. The number of layers was also estimated from the Raman spectroscopy mapping images of the graphene films at 532 nm in Figure 2c. The spectra contained three main peaks at ~ 1350 cm^{-1}, ~ 1585 cm^{-1}, and ~ 2690 cm^{-1}, which correspond to the D, G, and 2D peaks, respectively. The height ratio of the 2D to the G peaks (I_{2D}/I_G) is related to the graphene sheet thickness; for monolayer graphene, I_{2D}/I_G

> 2 and for bilayer graphene, $0.7 < I_{2D}/I_G < 1.3$.[29-32] All mappings indicated similar graphene

thickness distributions (Supporting Information, Figure S1). Monolayers covered 28.6%, 34.7%

and 32.9%, and bilayers covered 67.9%, 61.3% and 62.0% of the 1st, 3rd, and 5th Ni substrates,

respectively. Moreover, the height ratio of the D to the G peaks (I_D/I_G) is related to defect

density of the graphene sheet. All mappings indicated similar distributions for defect density

(Supporting Information, Figure S1).[31] Graphene on the stacked Ni films was transferred onto

glass substrates. Similarly to the properties of the graphene films obtained from the roll-

stacked system, the transmittance T of each film from multi-stacked system was found to be

approximately 90% at a wavelength of 550 nm, with a sheet resistance R_S of 4.3 kΩ/sq

averagely, as shown in Figure 2d. The obtained sheet resistance values were considered

reasonable regarding the previous reports on the graphene grown on Ni, which generally

show roughly 1 ~ 2 kΩ/sq for 80% transmittance.[13] Therefore, it is reasonable to consider all

the graphene films obtained in this system had similar properties except for the non-stacked

catalyst (0th layer). These results indicate that formation of graphene in the confined catalytic

geometry underwent different growth behavior, which could be ranging from dissolution of

carbonaceous species to the segregation and precipitation of dissolved carbon atoms in Ni.

3. Graphene growth in a confined geometry

To understand the variation in graphene growth under the confined catalytic geometry, the

differences between graphene growth in the stacked system and the non-stacked system were

investigated. Graphene growth requires two important steps: 1) dissolution of the carbon

source into the Ni surface, and 2) the segregation and precipitation of dissolved carbon atoms

on the surface.[33-35] One of the most important factors in the dissolution step is the number of

carbon atoms dissolved in the Ni film. In the segregation and precipitation step, the qualities of the Ni surface affect graphene film formation. The dissolution step decides the number of carbon atoms dissolved in the Ni film.

3.1. Carbon dissolution in a confined geometry: *Knudsen* molecular flow

In the conventional one-pot CVD process, the Ni surface is completely exposed to the gas flow, as is the case in the non-stacked system. To describe the mass transport of carbon sources to the catalytic surface in graphene growth, previous researchers have used the boundary layer theory of fluid mechanics.[22-25] The main assumption in this theory is the continuum flow where the fluids are regarded as undergoing continuous flow. However, as the gap between the stacks through which the flow passes becomes smaller, the system enters the non-continuum flow regime due to geometric restrictions. In the non-continuum regime, the fluid flow resembles discrete molecular motion because the viscous forces at the walls become dominant. Therefore, the mass transport of the source species for graphene growth is expected to alter significantly when the geometry becomes more confined and the flow regime changes. To characterize this phenomena, the *Knudsen* flow regime can be used to take into account the effects of the molecular mean-free-path λ and the system dimension d. The ratio, *Knudsen* number, $Kn = \lambda/d$, can be used to distinguish continuum flow from non-continuum flow. [36, 37]

Conventionally, $Kn < 0.001$ is the continuum flow regime with non-slip boundary conditions; $0.001 < Kn < 0.1$ is the continuum flow regime with slip boundary conditions; $0.1 < Kn < 10$ is a transition flow regime; $Kn > 10$ is a free molecular flow regime. Transition flow and free molecular flow are within the non-continuum flow regimes, in which each gas

molecule collide more often with the wall than with other gas molecules. The gas-gas collision only have minor effect on trajectory of gas molecules. Therefore, λ is then limited by the system dimension, which, in our system, can be described as the size of the gap between stacks, L.

Considering kinetic theory of gases, the collision frequency of gas molecules increases as the λ decreases. However, provided that the total pressure of the system is preserved, two open-ends of the gap result in decrement of the total number of gas molecules proportional to the decrement of gap size. Therefore, the total gas-wall collision frequency is similar regardless of the gap size. The most significant difference in the *Knudsen* flow regime is the diffusivity, D, of the molecules. Considering that the molecular diffusion is highly dependent on the collision of molecules, the relative diffusivity of the confined system, D_K, with respect to the open, non-stacked system, D_A, is then described by the following equation (see supporting information for details),

$$D_K = \frac{D_A}{Kn}$$

From the above relation, it can be easily inferred that the prolonged residence of gas molecules within the gap results in higher total collision density, therefore the probability of surface reaction and dissolution of carbon source into the Ni catalyst can dramatically increase as the *Knudsen* number increases. Once the number of dissolved carbon atoms is sufficient, graphene can form. This postulation is in good agreement with the results for the roll-stacked coil, in which graphene grows on Ni films facing the bare side of the SUS substrate, but not on the open catalytic surface, as already shown in Figure 1. More systematic investigations of *Knudsen* flow regime were performed by adjusting the gas flow

rates and gap sizes to properly address the importance of considering system dimension on graphene growth under the confined system.

Effects of the carbonaceous gas flow concentration

Firstly, we changed the gas flow rates during the CVD process in both the two-layer stacked system(with gap size of 135 nm) and the non-stacked system, (2 to 50 sccm; CH_4 concentration 0.33 vol% to 7.69 vol% with the flow rates in the proportion H_2:Ar = 100:500 sccm). Graphene films transferred onto the Si substrates consisted of multi-layer graphene sheets, as shown in Figures 3a ~ b, as observed for the multi-layer stacked system. In the stacked system, graphene grew even at CH_4 concentrations as low as 0.33 vol% (Figure 3a), while, in the non-stacked system, graphene did not grow at CH_4 concentrations until 10 times higher CH_4 concentration, 3.23 vol% (Figure 3b). The T and R_S values of the graphene films were measured after they were transferred onto glass substrates. Generally, R_S increases as the number of layers decreases.[38-40] As shown in the Figure 3c, the R_S of graphene obtained from the stacked system was higher than that of non-stacked graphene. At a wavelength of 550 nm, T was 88.5 ~ 90.5% for graphene from the two-layer stacked system but only 85.5 ~ 87.6% for graphene from the non-stacked system. The average R_S of graphene from the two-layer stacked system was 4.9 ~ 6.3 kΩ/sq (8.3 kΩ/sq for 0.33 vol% CH_4 flow) and that from the non-stacked system was 1.2 ~3.2 kΩ/sq. Interestingly, the values of R_S were remarkably reduced by properly adjusting the gap size in the stacked system (down to 1.6 kΩ/sq), while preserving the high transparency (T > 89%) (Figure 4c). These results indicate that other than the low-onset of graphene growth with respect to CH_4 concentration, the confined geometry

12

could also elevate the quality and homogeneity of the synthesized graphene films (discussed in detail in the section 3.2).

Raman spectra were taken from five locations of each graphene films grown under each condition (Supporting Information, Figure S2). The spectrum showed three main peaks at ~ 1350 cm^{-1}, ~ 1585 cm^{-1}, and ~ 2690 cm^{-1}, corresponding to D, G, and 2D peaks, respectively. The ratio of the 2D to G peaks (I_{2D}/I_G) indicated that single-, bi-, and multi-layer graphene sheets formed in various areas, and that the stacked system produced more mono- and bilayer sheets than did than the non-stacked system (Supporting Information, Figure S3).

Aside from the quality variation (will be explained in the later section), firstly, we investigated the criteria for the onset of graphene growth with respect to the CH$_4$ concentration. The *Knudsen* number of our stacked, confined system was estimated by calculating the mean free path as follows,

$$\lambda = \frac{k_B K}{\sqrt{2}\pi\sigma^2 p}$$

where,

k_B = Boltzmann constant [1.38 x 10^{-23} (kg·m^2/s^2)/K],

K = thermodynamic temperature [900 °C = 1173.15 K],

σ = particle hard shell diameter [diameter of CH$_4$ molecule = 0.38 nm],

and p = total pressure [1.6 Torr = 213.3 kg/(m·s^2)].

We calculated that $\lambda \approx 119$ μm and estimated that $L \approx 135$ nm because the upper substrate and the Ni film substrate are not perfectly flat: the maximum height of the Ni film surface was 69.7 nm after CVD and the height of the back side of the upper substrate was approximately 65 nm (Supporting information, Figure S4). In this system Kn = 881.5 which was well over 10, therefore, the gas flow through the gap is in the free molecular flow regime.

Furthermore, we estimated $L \approx 200$ nm in the roll-stacked system ($Kn = 595$), because the maximum height of the SUS surface was 130 nm (Supporting information, Figure S4). In case of hydrogen, which is already known to have minor effect on the dissolution step of graphene CVD growth on Ni,[41] it is expected to have relatively similar kinetic behavior to the non-stacked system due to much smaller molecular radius (0.12 nm) and consequently a shorter λ than methane. Therefore, together with the fact that only gas-wall collision is prevailed in *Knudsen* flow regime, it is reasonable to consider that the stacked system majorly affected the CH_4 gas flow which directly decided the resultant dissolution step.

In the stacked system, as indicated by large Kn, the diffusivity of CH_4 gas molecules within the gap channel was significantly enhanced, so that the increased dissolution of carbon species into Ni results in at least, considering instrumental allowance, 10 times lower CH_4 concentration for the onset of graphene growth (3.23 vol% to 0.33 vol%). It has been reported that the segregation limit (single and few layer graphene growth) of carbon concentration (c_s) in Ni is about 5.1×10^{20} carbon atoms/cm^3 at 900 ˚C.[34] Therefore, in non-stacked system, we can safely speculate that spontaneously dissolved carbon concentration in Ni film at 3.23 vol% CH_4 flow was near c_s. Since we used 400nm-thick Ni film at 3.23 vol% CH_4 flow, the dissolved carbon concentration per area of Ni was about 1.9×10^{16} carbon atoms/cm^2, which, considering atomic density of graphene (3.8×10^{15} carbon atoms/cm^2), corresponded to the areal density of approximately 5 homogeneous graphene layers.

In kinetic theory of gases, gas-wall collision frequency is directly proportional to the gas concentration. Therefore, 1/10 of gas flow, *i.e.* 0.33 vol% of CH_4 flow, only guaranteed 0.51 graphene layer in the non-stacked system, which was not sufficient to form even a single graphene layer. Surprisingly, in case of the stacked system, 0.33 vol% of CH_4 successfully

induced the formation of average 1.98 layers of fully covered graphene over the entire

catalytic surface, therefore indicating at least 10 times higher dissolution probability than

non-covered system. Furthermore, regarding the abundance of carbon source flow (5.4×10^{20}

molecules/10min, 2 sccm), it can also be expected that rather precipitation (amorphous

carbon growth) than segregation could have occurred in the stacked system at given large

Knudsen number.[34, 41] However, up until 7.69 vol% (50 sccm) CH_4 flow, no precipitation

occurred for both the stacked and non-stacked system. The limited number of CH_4 molecules

due to small gap, assuming homogeneous gas flux for both inside and outside the gap, would

have suppressed the overdose of dissolved carbon in Ni. From above results, it can be

reasonably concluded that the increased carbon dissolution probability of the stacked system

only give rise to sufficient carbon concentration for the growth of graphene, rather than for

precipitation of amorphous carbon. Moreover, considering inhomogeneous dissolved-carbon

distribution across the Ni grain boundaries, the graphene growth would have been spurred by

the possible change in the morphology of Ni surfaces. However, the increased portion of (111)

crystalline plane, enlarged grain size, and decreased surface roughness (Figure 5) in the

stacked system indicate that low CH_4 concentration for the onset of graphene growth could

not be promoted by surface characteristics of Ni. These change rather enhanced the quality

(distribution of number of layers) of synthesized graphene. This will be discussed in detail in

the section 3.2.

Effects of the gap size variation

So far, we successfully assessed the variation in dissolution probability by introducing

Knudsen flow regime. As a next step, we systematically varied the *Knudsen* number and

investigated its effect on graphene growth by directly varying gap sizes in the range 135 nm <

L < 1.2 mm; λ = 119 μm was fixed for the CH_4 flow. A gas mixture containing 1.64 vol% of

CH_4 concentration was passed through the gap, and the CVD chamber was heated to 900°C.

When L = 10 μm, Kn = 11.9, so the gas flow was in the free molecular flow regime; when L

> 1.2 mm, Kn < 0.01, so the flow was in the slip flow regime; when 10 μm < L < 1.2 mm, the

flow was in the transition flow regime (Supporting Information, Table S1). From the results

in previous section, it was safe to expect that 5 times larger gap size than minimum gap (135

nm, Kn = 881.5) would be sufficient to spur the growth of graphene at this CH_4 concentration.

In theory, Kn of at least 2 was required to provide dissolved carbon concentration above the

segregation limit in the stacked system at 1.64 vol% CH_4 flow. However, as the Kn decreased

under 10 ~ 0.1, as in transition regime, the diffusion of gas molecules was no longer solely

limited by gas-wall collision, but also affected by presence of other gas molecules. The

cumulative contribution of both collisions decides the overall diffusivity of gas molecules.

Therefore, in the transition regime, it can be deduced that the diffusivity becomes lower than

expectation from extension of free-molecular flow.

In our system, graphene films were formed for L < 600 μm (Kn > 0.2) (Figure 4a) of which

the T at 550 nm was ~ 90%, and R_s was 1.8 ~ 4.8 kΩ/sq (Figure 4b). Graphene grew in both

the free molecular flow regime (135 nm < L < 10 μm) and the transition flow regime (30 μm

< L < 600 μm), but not in the slip flow regime (L = 1.2 mm), as shown in Figures 4a, b.

Therefore, the relative criteria for graphene growth at 10 sccm (1.64 vol%) of CH_4 flow was

Kn > 0.1, just within the boundary of transition flow regime. Considering the similar

estimated dimensions of geometric confinement in the roll-staked (200nm) and the simple

stacked (135nm) systems, the *Knudsen* number of the roll-stacked system also satisfactorily

met the criteria for the graphene growth, which agreed well with the observed graphene

growth behaviors in section 1 and 2.

Although these analyses based on *Knudsen* molecular flow explained the overall trends in

graphene growth, the quality of graphene could not be estimated by only *Knudsen* flow

theory. It is well known that the quality of graphene is mainly decided by the segregation and

precipitation step rather than the dissolution step, provided that dissolved carbon

concentration is well within the window the segregation limit.[34] As mentioned earlier, the

limited amount of maximum dissolved carbon in 400nm Ni was well within the segregation

limit, so that the difference in graphene quality (Figure 5, Figure S3) mainly originated from

the variation in the segregation and precipitation step.

3.2. Segregation and precipitation step

In the segregation and precipitation step, the rate of temperature cooling and the metal

surface properties have critical influences, because they determine the number of layers in

CVD-grown graphene.[42-48] To reduce the amount of multi-layer graphene, the number of

grain boundaries in the polycrystalline Ni films should be decreased, because the dissolved

carbon atoms in the Ni films easily come out through the grain boundaries and form the

multi-layer graphene.[44, 45] In addition, the proportion of the (111) plane should be increased in

the polycrystalline Ni films.[46-48] In the stacked system, the stack might induce change in

crystallographic or/and morphological properties of the Ni catalyst, which could exert large

influence on segregated graphene quality. Moreover, as briefly mentioned in section 3.1, it is

worth pointing out that the change of surface characteristics can also affect the segregation

limit of carbon concentration, considering the possible increment in the inhomogeneity of

carbon distribution across the grain boundaries. In this sense, we carefully examined the morphological and crystallographic characteristics of the Ni surfaces.

Morphology of Ni surfaces

Figure 5a ~ b shows the quality of graphene under the stacked system. It is clear that distribution of I_{2D}/I_G in the stacked system had larger domains and was more dedicated to higher values, which indicated homogeneous and monolayer growth of graphene. As mentioned before, the graphene quality, *i.e.* homogeneity and relative portion of monolayer graphene, is mainly decided by the segregation and precipitation step, which is influenced by surface morphology and crystallographic orientation of Ni surfaces. Atomic force microscopy (AFM) was used to examine the Ni film surface to determine how the quality of the Ni film after annealing under low-pressure H_2/Ar affects graphene synthesis. AFM images of an evaporated Ni film were obtained prior to heat treatment (Figure 5c), and after annealing the Ni surfaces in the stacked system (Figure 5d) and in the non-stacked system (Figure 5e). After annealing at 900°C, the surface roughness (RMS) of the stacked system was 8.7 nm and that of the non-stacked system was 23.8 nm. The maximum height of the Ni films in the stacked system was 69.7 nm and that of the non-stacked system was 270.9 nm. In the images, it can be seen that the grains were larger and smoother in the stacked system than in the non-stacked system; *i.e.*, the Ni surfaces of the stacked system were flatter and had fewer grain boundaries than the non-stacked system; stacking the substrates resulted in the flattening of the Ni crystals due to the external strain physical confinement, which reduced the evaporative loss of metal.[49, 50] Decreasing the number of grain boundaries and smoothing the Ni surface might reduce the amount of multi-layer graphene, which increased the transmittance *T* of graphene. As the gap size increased, the surfaces became gradually rough, but still showed

smooth domains without any development of small spike-like features as in non-stacked systems (Supporting Information, Figure S5). After annealing, the Ni surface for a gap size of 30 μm has RMS = 17.4 nm and maximum height = 137.2 nm, and for a gap size of 1.2 mm RMS = 24.1 nm and the maximum height = 170.3 nm. These results agreed well with the measured average sheet resistance Rs of graphene films obtained by adjusting the gap size, which was around 2.3 kΩ/sq at T of 89.4 %, as shown in Figure 4b. With smoother grains, the synthesized graphene films were not only transparent but also highly conductive. Increasing the gap size slightly increased the R_S up to 3 kΩ/sq, but still preserved high T above 90%, indicating higher homogeneity of graphene films synthesized under the stacked system than the non-stacked system. For the closely stacked system (135nm gap), the slightly higher measured R_S (4.9 kΩ/sq) could be resulted from the physical interruption of graphene growth on the Ni surface contacted with the upper substrate, and possibly from the increased etching of carbon species by significantly reduced the H_2 diffusion rate at the smallest gap. Electron backscattered diffraction (EBSD) also indicated that the stacked system had larger grains with a larger range of sizes than the non-stacked system, as could be seen in Figure 5f. Thus, the stacked system had fewer grain boundaries than the non-stacked system.

Clearly, the introduction of the confined catalytic geometry promoted reduction in the surface roughness and decrement in the number of grain boundaries of the Ni catalyst as the gap narrowed. These variations in Ni surface resulted in enhancement of graphene quality by reducing graphene nucleation sites such as grain boundaries and defects. Moreover, since these reduction generally increased the segregation limit on carbon concentration, the growth of graphene even at low CH_4 concentration (0.33 vol%) in the stacked system conclusively

eliminated the possibility that the change of Ni morphology promoted the onset of graphene growth at low CH_4 concentration in the stacked system, as suggested earlier in the section 3.1.

Crystallographic characteristics of Ni

The annealed Ni surfaces were examined to determine how their crystallographic characteristics affect the synthesized graphene films. Increases in the (111) peak intensity and in the (111) grain size of the Ni films increase the probability that graphene will form either monolayers or bilayers.[46, 47] Crystalline orientation maps for the normal direction of the Ni films were obtained with EBSD. Three grain orientations, (111), (001), and (101) were evident in Figures 5c' ~ e'. The EBSD mapping of the as-evaporated Ni film surface prior to heat treatment indicated that there were no specific crystalline domains, as shown in Figure 5c'. However, specific crystalline domains developed after heat treatment. The crystalline domains were larger in the stacked system (Figure 5d') than in the non-stacked system (Figure 5e'). As the crystalline domains developed, the (111) directions developed effectively in the stacked system, but no preferred orientation was evident in the non-stacked system. The out of-plane X-ray diffraction patterns of the three Ni films also showed that there was no preferred intensity of reflections in the as-evaporated Ni film, but there were large increases in the intensities of the (111) reflections at $q = 3.07$ nm^{-1} after thermal annealing, as shown in Figure 5g. However, during the annealing process, the crystallinity of (111) plane of the Ni surface in the stacked system increased; the intensity of the (111) peak was twice as high in the stacked system as in the non-stacked system. As a result, the crystal orientation of the stacked Ni surface increased in the proportions of mono- and bilayer graphene (Figure 5a, b and Figure S3). These observations also agreed well with the previous results, as in Ni morphology and graphene quality.

4. Application of roll-synthesized graphene

The development of flexible transparent conducting films (TCFs) is a key to the realization of flexible electronics. The graphene-based TCFs have intrinsic flexibility and transparency along with high electrical properties, which makes graphene TCF a highly feasible flexible TCF for real application[51]. In this sense, a low-energy consuming, high-throughput production of graphene sheet is a basic step toward the soft electronics. To demonstrate the applicability of our method, we fabricated graphene based flexible TCFs and flexible organic field effect transistor (OFET) array on plastic. We could obtain 8 cm × 3 cm (width × length) flexible graphene TCFs on PET film via the one-pot CVD synthesis based on the roll-stacked catalytic coil with effective dimension of 1 cm × 3 cm (diameter × length), which increased the productivity of graphene synthesis by almost one order. We also demonstrated pentacene based organic transistor on plastic using pattern-transferred graphene as source/drain electrodes. The device showed stable operation with hole mobility of 0.51 cm^2/Vs and high mechanical stability. (Supporting Information, Figure S6)

Conclusions

We have demonstrated a high-throughput CVD synthesis of graphene on polycrystalline Ni films by using a roll-stacked catalytic coil, and systematically studied the graphene growth mechanism on confined catalytic substrates. Graphene was successfully synthesized at very low CH$_4$ concentrations in a confined geometry, of which the gas flow was characterized as the free molecular flow and transition flow regimes ($Kn > 0.1$). Moreover, the confined

21

geometry also altered the evolution of the morphological and crystallographic structure of the Ni films during the CVD process. Reducing the gap size increased the size of the Ni grains and promoted the predominant development of (111) crystal orientation on the surface of the Ni catalyst. As a consequence, the proportion of mono- and bilayer components of the graphene film was increased and the number of graphene layer showed narrow distribution, which resulted in the increased homogeneity of the synthesized graphene sheets.

This work provides a simple and efficient method to maximize the catalytic area without unnecessary time and energy consumption. Moreover, we believe that the controlled evolution of the catalytic surface in our work might provide a new avenue for high quality and large-area graphene synthesis, which possesses high feasibility for a wide range of applications such as soft electronics based on both organic semiconductor and graphene electrodes.

Acknowledgement

Figure captions

Figure 1. (a) A roll-stacked Ni coil before and after the CVD process. (b) Schematic diagram of a roll-stacked coil and an image of CVD-grown graphene transferred onto a glass substrate. (c) Optical images of graphene transferred onto a SiO_2/Si wafer from a roll-stacked Ni coil.

Figure 2. (a) Schematic diagram of the multi-layer stacked Ni substrates for the CVD-grown graphene. (b) Optical images and (c) Raman 2D-mappings of the graphene films obtained from the multi-layer stacked substrates, 0th, 1st, 3rd, and 5th layers (I_{2D}/I_G, area 400 μm^2). (d) Transmittances and sheet resistances of the graphene films obtained from the multi-layer stacked substrates. Dotted lines indicate the average values of transmittance and sheet resistance.

Figure 3. Optical images of graphene films transferred onto SiO_2/Si wafers (a) grown in the bi-layer stacked system under various CH_4 concentrations, 0.33 ~ 7.69 vol%, and (b) grown in the non-stacked system under various CH_4 concentrations, 0.33 ~ 7.69 vol%. (c) Transmittances and sheet resistances of graphene obtained at each CH_4 concentration. Dotted lines indicate the average values of transmittance and sheet resistance.

Figure 4. (a) Optical images of graphene films transferred onto SiO_2/Si wafers after synthesis with gaps in the range 135 nm ~ 1.2 mm. (b) Transmittances and sheet resistances of CVD-grown graphene. Dotted lines indicate the average values of transmittance and sheet resistance. (c) Schematic diagram of the flow regimes.

Figure 5. (a) Statistical distribution and (b) 2D-mapping image of Raman I_{2D}/I_G ratio of graphene films synthesized in the bi-layer stacked and non-stacked system under 4.76 vol% of CH_4 concentration (area 100 μm^2). AFM images of (c) an as-evaporated Ni surface and Ni surfaces heat-treated under a H_2/Ar atmosphere in (d) stacked and (e) non-stacked systems. (f) Grain size distributions for heat-treated Ni films obtained with EBSD. Normal-directional EBSD mapping of (c') the as-evaporated Ni surface and the Ni surfaces thermally treated under a H_2/Ar atmosphere of the (d') stacked and (e') non-stacked systems. The colors represent the orientations of the polycrystalline Ni films after heat treatment. (g) XRD spectra; the inset shows the (111) peak.

24

Notes and references

1. C. Lee, X. D. Wei, J. W. Kysar and J. Hone, *Science*, 2008, **321**, 385-388.

2. A. A. Balandin, *Nat Mater*, 2011, **10**, 569-581.

3. T. G. Pedersen, C. Flindt, J. Pedersen, A. P. Jauho, N. A. Mortensen and K. Pedersen, *Phys Rev B*, 2008, **77**, 245431.

4. W. H. Lee, J. Park, Y. Kim, K. S. Kim, B. H. Hong and K. Cho, *Adv Mater*, 2011, **23**, 3460-3464.

5. Y. W. Tan, Y. Zhang, K. Bolotin, Y. Zhao, S. Adam, E. H. Hwang, S. Das Sarma, H. L. Stormer and P. Kim, *Phys Rev Lett*, 2007, **99**, 246803.

6. S. Adam, E. H. Hwang, V. M. Galitski and S. Das Sarma, *P Natl Acad Sci USA*, 2007, **104**, 18392-18397.

7. H. H. Kim, J. W. Yang, S. B. Jo, B. Kang, S. K. Lee, H. Bong, G. Lee, K. S. Kim and K. Cho, *Acs Nano*, 2013, **7**, 1155-1162.

8. K. S. Novoselov, A. K. Geim, S. V. Morozov, D. Jiang, Y. Zhang, S. V. Dubonos, I. V. Grigorieva and A. A. Firsov, *Science*, 2004, **306**, 666-669.

9. K. V. Emtsev, A. Bostwick, K. Horn, J. Jobst, G. L. Kellogg, L. Ley, J. L. McChesney, T. Ohta, S. A. Reshanov, J. Rohrl, E. Rotenberg, A. K. Schmid, D. Waldmann, H. B. Weber and T. Seyller, *Nat Mater*, 2009, **8**, 203-207.

10. W. A. d. Heer and C. Berger, *J. Phys. D: Appl. Phys.*, 2012, **45**, 150301.

11. C. Riedl, C. Coletti and U. Starke, *J. Phys. D: Appl. Phys.*, 2010, **43**, 374009.

12. J. Hwang, M. Kim, D. Campbell, H. A. Alsalman, J. Y. Kwak, S. Shivaraman, A. R. Woll, A. K. Singh, R. G. Hennig, S. Gorantla, M. H. Rummeli and M. G. Spencer, *Acs Nano*, 2013, **7**, 385-395.

13. K. S. Kim, Y. Zhao, H. Jang, S. Y. Lee, J. M. Kim, K. S. Kim, J.-H. Ahn, P. Kim, J.-Y. Choi and B. H. Hong, *Nature*, 2009, **457**, 706-710.

14. G. Faggio, A. Capasso, G. Messina, S. Santangeo, T. Dikonimos, S. Gagliardi, R. Giorgi, V. Morandi, L. Ortolani and N. Lisi, *J Phys Chem C*, 2013, **117**, 21569-21576.

15. H. Kim, I. Song, C. Park, M. Son, M. Hong, Y. Kim, J. S. Kim, H.-J. Shin, J. Baik and H. C. Choi, *Acs Nano*, 2013, **7**, 6575-6582.

16. S. Bae, H. Kim, Y. Lee, X. Xu, J. S. Park, Y. Zheng, J. Balakrishnan, T. Lei, H. Ri Kim, Y. I. Song, Y. J. Kim, K. S. Kim, B. Özyilmaz, J. H. Ahn, B. H. Hong and S. Iijima, *Nat. Nanotechnol.*, 2010, **5**, 574-578.

17. C. D. Liao, Y. Y. Lu, S. R. Tamalampudi, H. C. Cheng and Y. T. Chen, *J Phys Chem A*, 2013, **117**,

Nanoscale Accepted Manuscript

9454-9461.

18. L. David, R. Bhandavat, G. Kulkarni, S. Pahwa, Z. Zhong and G. Singh, *Acs Appl Mater Inter*, 2013, **5**, 546-552.

19. T. Kobayashi, M. Bando, N. Kimura, K. Shimizu, K. Kadono, N. Umezu, K. Miyahara, S. Hayazaki, S. Nagai, Y. Mizuguchi, Y. Murakami and D. Hobara, *Appl. Phys. Lett.*, 2013, **102**, 023112.

20. Y. Zhang, L. Zhang, P. Kim, M. Ge, Z. Li and C. Zhou, *Nano Lett.*, 2012, **12**, 2810-2816.

21. M. H. Rümmeli, S. Gorantla, A. Bachmatiuk, J. Phieler, N. Geißler, I. Ibrahim, J. Pang and J. Eckert, *Chem. Mater.*, 2013, Online published.

22. C. Jia, J. Jiang, L. Gan and X. Guo, *Sci. Rep.*, 2012, **2**, 1-6.

23. S. Bhaviripudi, X. T. Jia, M. S. Dresselhaus and J. Kong, *Nano Lett.*, 2010, **10**, 4128-4133.

24. A. M. Lewis, B. Derby and I. A. Kinloch, *Acs Nano*, 2013, **7**, 3104-3117.

25. S.-Y. Cho, K.-J. Kim, H.-M. Kim, D.-J. Lee, M.-H. Lee and K.-B. Kim, *RSC Adv.*, 2013, **3**, 26376-26381.

26. M. G. Rybin, A. S. Pozharov and E. D. Obraztsova, *Phys. Status Solidi C*, 2010, **7**, 2785-2788.

27. J. J. Lander, H. E. Kern and A. L. Beach, *J. Appl. Phys.*, 1952, **23**, 1305-1309.

28. C. M. Nolen, G. Denina, D. Teweldebrhan, B. Bhanu and A. A. Balandin, *Acs Nano*, 2011, **5**, 914-922.

29. K. Yan, H. L. Peng, Y. Zhou, H. Li and Z. F. Liu, *Nano Lett.*, 2011, **11**, 1106-1110.

30. Z. Yan, Z. W. Peng, Z. Z. Sun, J. Yao, Y. Zhu, Z. Liu, P. M. Ajayan and J. M. Tour, *Acs Nano*, 2011, **5**, 8187-8192.

31. A. C. Ferrari, J. C. Meyer, V. Scardaci, C. Casiraghi, M. Lazzeri, F. Mauri, S. Piscanec, D. Jiang, K. S. Novoselov, S. Roth and A. K. Geim, *Phys Rev Lett*, 2006, **97**, 187401.

32. J. Lee, K. S. Novoselov and H. S. Shin, *Acs Nano*, 2011, **5**, 608-612.

33. X. S. Li, W. W. Cai, L. Colombo and R. S. Ruoff, *Nano Lett.*, 2009, **9**, 4268-4272.

34. L. Baraton, Z. B. He, C. S. Lee, C. S. Cojocaru, M. Chatelet, J. L. Maurice, Y. H. Lee and D. Pribat, *EPL*, 2011, **96**, 46003.

35. R. S. Weatherup, B. C. Bayer, R. Blume, C. Baehtz, P. R. Kidambi, M. Fouquet, C. T. Wirth, R. Schlogl and S. Hofmann, *Chemphyschem*, 2012, **13**, 2544-2549.

36. K. Xu and Z. H. Li, *J. Fluid Mech.*, 2004, **513**, 87-110.

37. D. A. Nield and A. V. Kuznetsov, *Transp. Porous Med.*, 2006, **64**, 161-170.

38. D. Y. Wan, T. Q. Lin, H. Bi, F. Q. Huang, X. M. Xie, I. W. Chen and M. H. Jiang, *Adv Funct Mater*, 2012, **22**, 1033-1039.

39. S. S. Chen, W. W. Cai, R. D. Piner, J. W. Suk, Y. P. Wu, Y. J. Ren, J. Y. Kang and R. S. Ruoff,

Nano Lett., 2011, **11**, 3519-3525.

40. G. Jo, M. Choe, S. Lee, W. Park, Y. H. Kahng and T. Lee, *Nanotechnology*, 2012, **23**, 112001.

41. M. Losurdo, M. M. Giangregorio, P. Capezzuto and G. Bruno, *Phys Chem Chem Phys*, 2011, **13**, 20836-20843.

42. K. Xiao, H. Wu, H. Lv, X. Wu and H. Qian, *Nanoscale*, 2013, **5**, 5524-5529.

43. Q. Yu, J. Lian, S. Siriponglert, H. Li, Y. P. Chen and S.-S. Pei, *Appl. Phys. Lett.*, 2008, **93**, 113103.

44. Y. Zhang, L. Gomez, F. N. Ishikawa, A. Madaria, K. Ryu, C. A. Wang, A. Badmaev and C. W. Zhou, *J. Phys. Chem. Lett.*, 2010, **1**, 3101-3107.

45. Y. Xue, B. Wu, Y. Guo, L. Huang, L. Jiang, J. Chen, D. Geng, Y. Liu, W. Hu and G. Yu, *Nano Res.*, 2011, **4**, 1208-1214.

46. J. Wintterlin and M. L. Bocquet, *Surf. Sci.*, 2009, **603**, 1841-1852.

47. S. Thiele, A. Reina, P. Healey, J. Kedzierski, P. Wyatt, P. L. Hsu, C. Keast, J. Schaefer and J. Kong, *Nanotechnology*, 2010, **21**, 015601.

48. S. J. Kim, D. W. Kim and H. T. Jung, *RSC Adv.*, 2013, **3**, 22909-22913.

49. C. A. Volkert and C. Lingk, *Appl. Phys. Lett.*, 1998, **73**, 3677-3679.

50. A. M. Deus, M. A. Fortes, P. J. Ferreira and J. B. V. Sande, *Acta Mater.*, 2002, **50**, 3317-3330.

51. S. B. Jo, J. Park, W. H. Lee, K. Cho and B. H. Hong, *Solid State Communications*, 2012, **152**, 1350-1358.
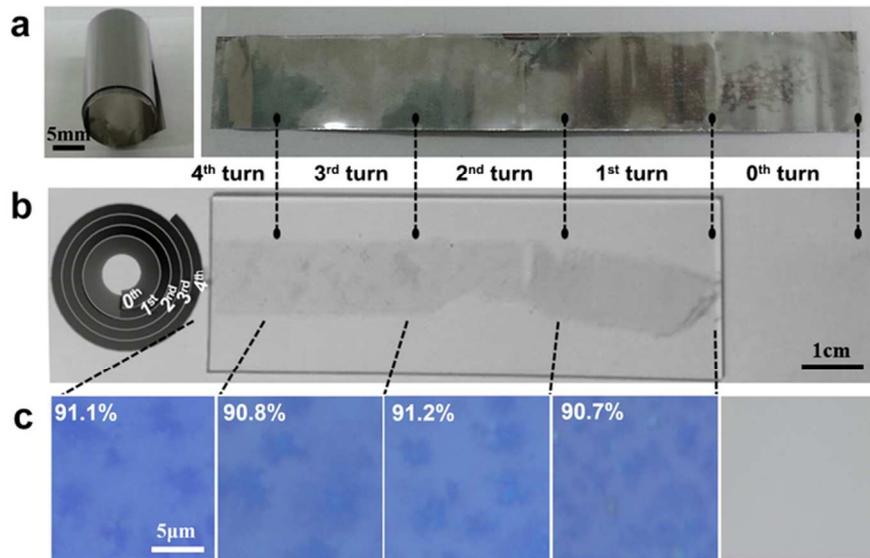
Figure 1. (a) A roll-stacked Ni coil before and after the CVD process. (b) Schematic diagram of a roll-stacked coil and an image of CVD-grown graphene transferred onto a glass substrate. (c) Optical images of graphene transferred onto a SiO_2/Si wafer from a roll-stacked Ni coil.
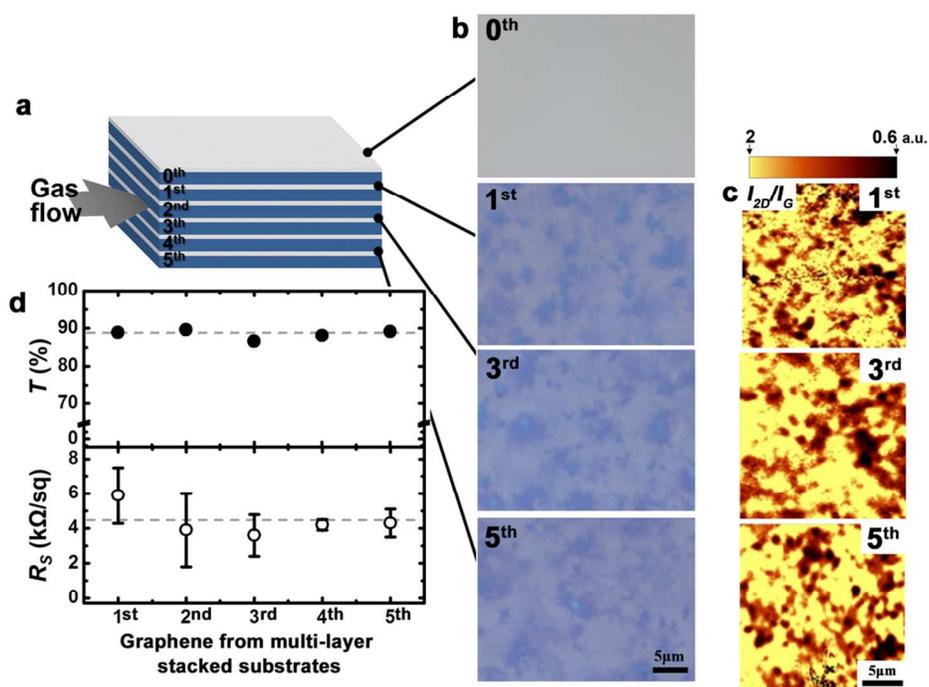
69x40mm (300 x 300 DPI)

Figure 2. (a) Schematic diagram of the multi-layer stacked Ni substrates for the CVD-grown graphene. (b) Optical images and (c) Raman 2D-mappings of the graphene films obtained from the multi-layer stacked substrates, 0th, 1st, 3rd, and 5th layers (I_{2D}/I_G, area 400 μm^2). (d) Transmittances and sheet resistances of the graphene films obtained from the multi-layer stacked substrates. Dotted lines indicate the average values of transmittance and sheet resistance.
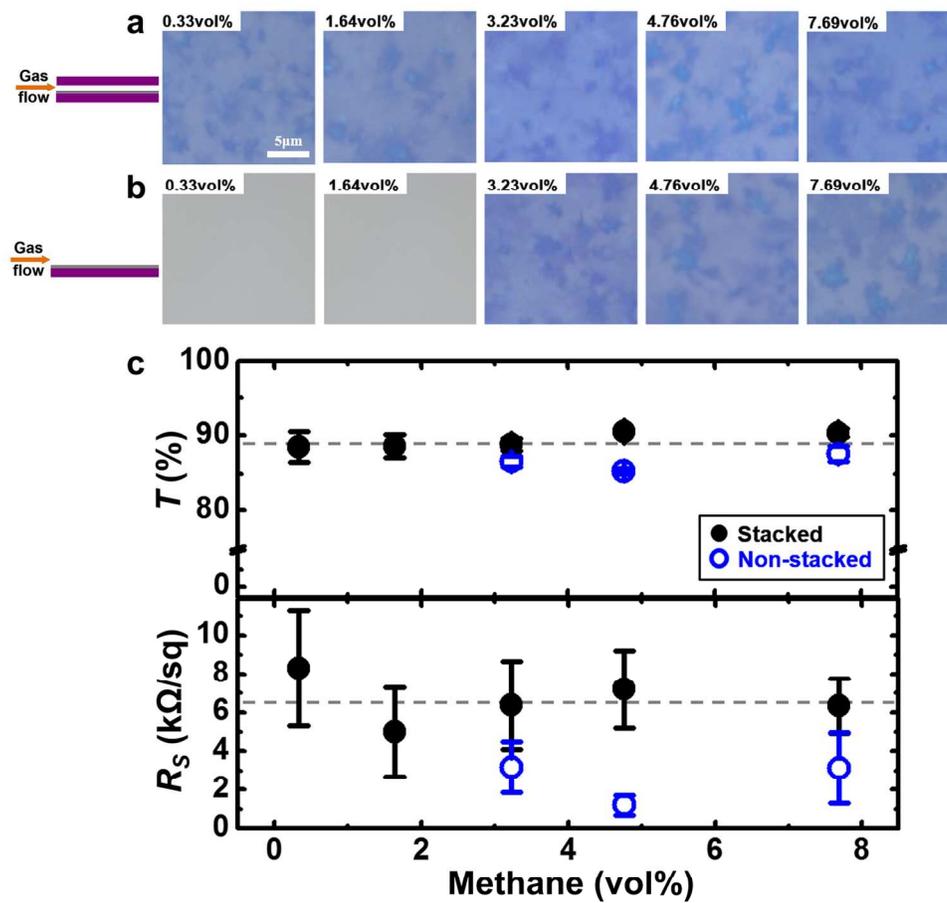
101x71mm (300 x 300 DPI)

Figure 3.Optical images of graphene films transferred onto SiO_2/Si wafers (a) grown in the bi-layer stacked system under various CH_4 concentrations, 0.33 ~ 7.69 vol%, and (b) grown in the non-stacked system under various CH_4 concentrations, 0.33 ~ 7.69 vol%. (c) Transmittances and sheet resistances of graphene obtained at each CH_4 concentration. Dotted lines indicate the average values of transmittance and sheet resistance.
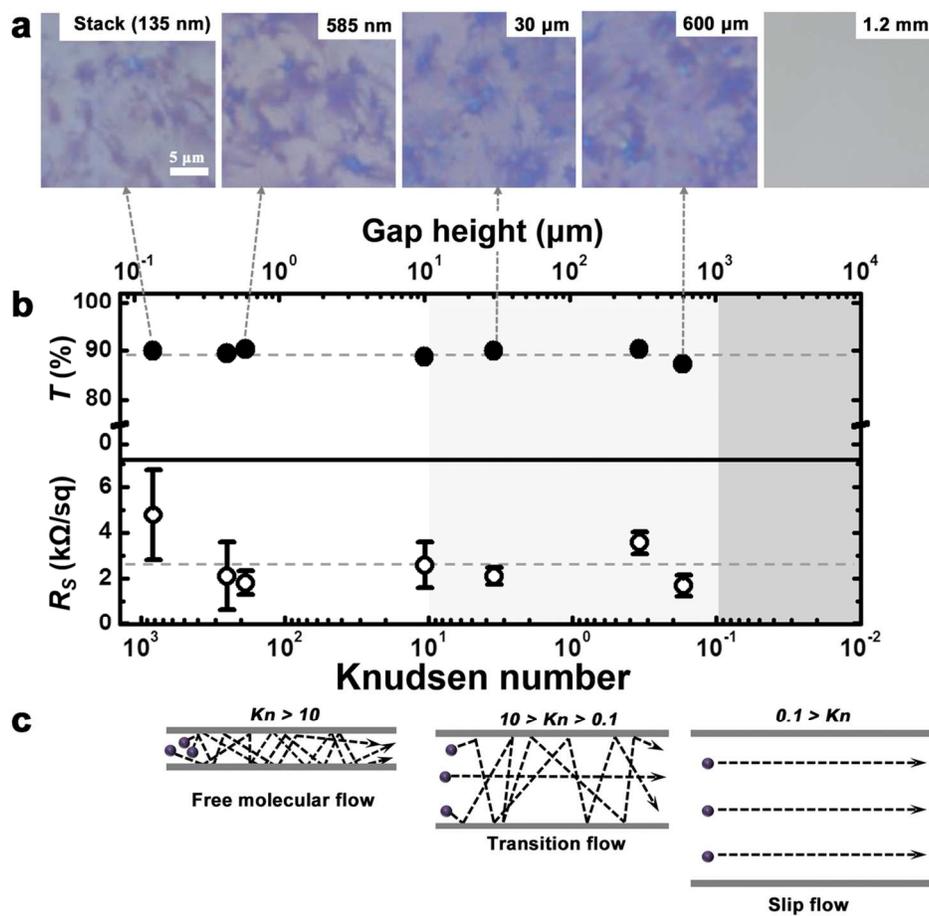144x142mm (300 x 300 DPI)

Figure 4. (a) Optical images of graphene films transferred onto SiO₂/Si wafers after synthesis with gaps in the range 135 nm ~ 1.2 mm. (b) Transmittances and sheet resistances of CVD-grown graphene. Dotted lines indicate the average values of transmittance and sheet resistance. (c) Schematic diagram of the flow regimes.
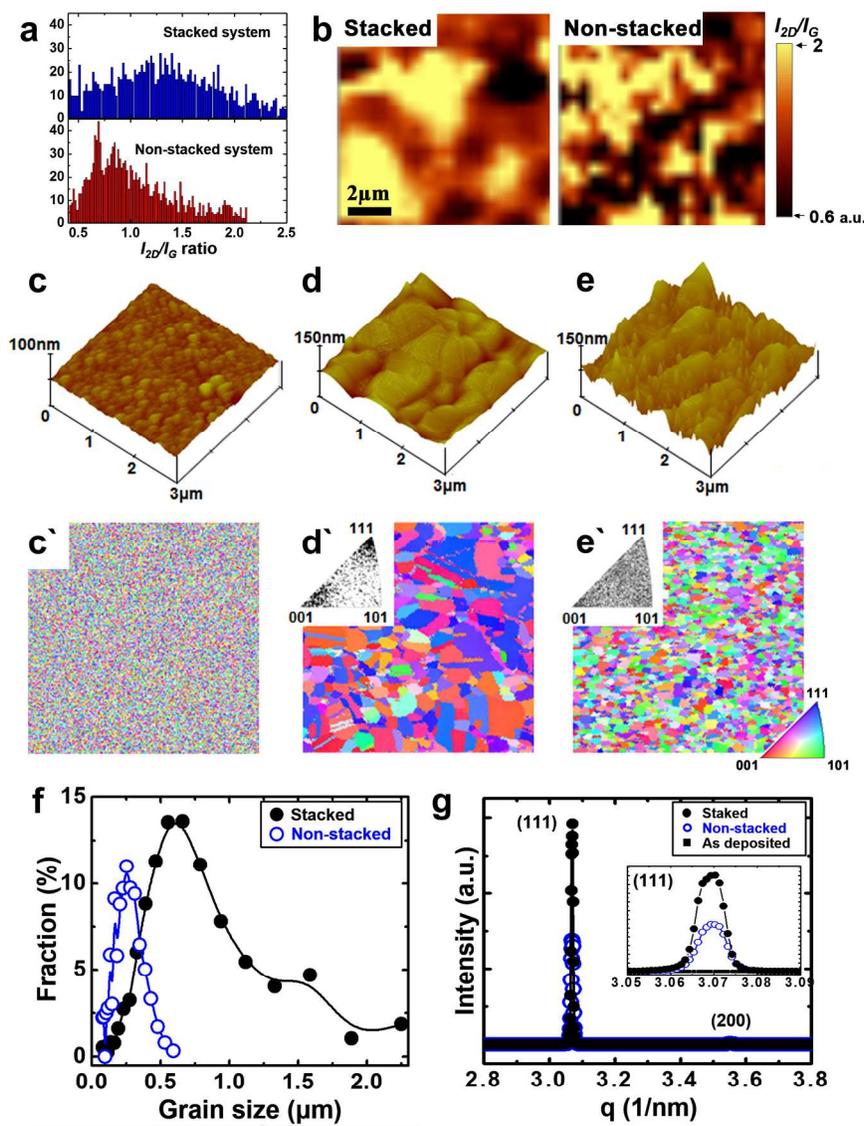
123x115mm (300 x 300 DPI)

Figure 5. (a) Statistical distribution and (b) 2D-mapping image of Raman I_{2D}/I_G ratio of graphene films synthesized in the bi-layer stacked and non-stacked system under 4.76 vol% of CH_4 concentration (area 100 μm^2). AFM images of (c) an as-evaporated Ni surface and Ni surfaces heat-treated under a H_2/Ar atmosphere in (d) stacked and (e) non-stacked systems. (f) Grain size distributions for heat-treated Ni films obtained with EBSD. Normal-directional EBSD mapping of (c') the as-evaporated Ni surface and the Ni surfaces thermally treated under a H_2/Ar atmosphere of the (d') stacked and (e') non-stacked systems. The colors represent the orientations of the polycrystalline Ni films after heat treatment. (g) XRD spectra; the inset shows the (111) peak.
191x251mm (300 x 300 DPI)